The landscape of human mutually exclusive splicing

Klas Hatje[1,2,#,*], Ramon O. Vidal[2,*], Raza-Ur Rahman[2], Dominic Simm[1,3], Björn Hammesfahr[1,$], Orr Shomroni[2], Stefan Bonn[2§] & Martin Kollmar[1§]

[1] Group of Systems Biology of Motor Proteins, Department of NMR-based Structural Biology, Max-Planck-Institute for Biophysical Chemistry, Göttingen, Germany

[2] Group of Computational Systems Biology, German Center for Neurodegenerative Diseases, Göttingen, Germany

[3] Theoretical Computer Science and Algorithmic Methods, Institute of Computer Science, Georg-August-University Göttingen, Germany

§ Corresponding authors

Current address: Roche Pharmaceutical Research and Early Development, Pharmaceutical Sciences, Roche Innovation Center Basel, F. Hoffmann-La Roche Ltd., Basel, Switzerland

$ Current address: Research and Development - Data Management (RD-DM), KWS SAAT SE, Einbeck, Germany

* These authors contributed equally

E-mail addresses:

KH: klas.hatje@roche.com, RV: ramon.vidal@dzne.de, RR: raza-ur.rahman@dzne.de, DS: dominic.simm@cs.uni-goettingen.de, BH: bjoern.hammesfahr@kws.com, OS: orr.shomroni@dzne.de, SB: stefan.bonn@dzne.de, MK: mako@nmr.mpibpc.mpg.de

Abstract

Mutually exclusive splicing of exons is a mechanism of functional gene and protein diversification with pivotal roles in organismal development and diseases such as Timothy syndrome, cardiomyopathy and cancer in humans. In order to obtain a first genome-wide estimate of the extent and biological role of mutually exclusive splicing in humans we predicted and subsequently validated mutually exclusive exons (MXEs) using 515 publically available RNA-seq datasets. Here, we provide evidence for the expression of over 855 MXEs, 42% of which represent novel exons, increasing the annotated human mutually exclusive exome more than five-fold. The data provides strong evidence for the existence of large and multi-cluster MXEs in higher vertebrates and offers new insights into MXE splicing mechanics and evolution. Finally, MXEs are significantly enriched in pathogenic mutations and their spatio-temporal expression predicts human disease pathology.

Introduction

Alternative splicing of pre-messenger RNAs is a mechanism common to almost all eukaryotes to generate a plethora of protein variants out of a limited number of genes (Matlin *et al*, 2005; Nilsen & Graveley, 2010; Lee & Rio, 2015). High-throughput studies suggested that not only 95-100% of all multi-exon genes in human are affected (Wang *et al*, 2008; Pan *et al*, 2008; Gerstein *et al*, 2014) but also that alternative splicing patterns strongly diverged between vertebrate lineages implying a pronounced role in the evolution of phenotypic complexity (Merkin *et al*, 2012; Barbosa-Morais *et al*, 2012). Five types of alternative splicing have been identified to contribute to most mRNA isoforms, which are differential exon inclusion (exon skipping), intron retention, alternative 5' and 3' exon splicing, and mutually exclusive splicing (Nilsen & Graveley, 2010; Wang *et al*, 2008; Pan *et al*, 2008; Blencowe, 2006). Mutually exclusive splicing generates alternative isoforms by retaining only one exon of a cluster of neighbouring internal exons in the mature transcript and is a sophisticated way to modulate protein function (Letunic *et al*, 2002; Meijers *et al*, 2007; Pohl *et al*, 2013; Tress *et al*, 2016). The most extreme cases known so far are the arthropod *DSCAM* genes, for which up to 99 mutually exclusive exons (MXEs) spread into four clusters were identified (Schmucker *et al*, 2000; Lee *et al*, 2010; Pillmann *et al*, 2011).

Opposed to arthropods, vertebrate MXEs have been reported to only occur in pairs (Matlin *et al*, 2005; Gerstein *et al*, 2014; Abascal *et al*, 2015a), and genome-wide estimates in human range from 118 (Suyama, 2013) to at most 167 cases (Wang *et al*, 2008). Despite these relatively few reported cases, mutually exclusive splicing might be far more frequent in humans than currently anticipated, as has been recently revealed in the model organism *D.melanogaster* (Hatje & Kollmar, 2013). Apart from their low number, MXEs have been described in many crucial and essential human genes such as in the α-subunits of six of the ten voltage-gated sodium channels (*SCN* genes) (Copley, 2004), in each of the glutamate

receptor subunits 1-4 (*GluR1-4*) where the MXEs are called flip and flop (Sommer *et al*, 1990), and in *SNAP-25* as part of the neuroexocytosis machinery (Johansson *et al*, 2008). Although MXEs within a cluster often share high similarity at the sequence level, they are usually not functionally redundant, as their inclusion in the mRNAs is tightly regulated. Thus, mutations in MXEs have been shown to cause diseases such as Timothy syndrome (missense mutation in the *CACNA1C* gene) (Splawski *et al*, 2004, 2005), cardiomyopathy (defect of the mitochondrial phosphate carrier *SLC25A3*) (Mayr *et al*, 2011) or cancer (mutations in e.g. the pyruvate kinase *PKM* and the zinc transporter *SLC39A14*) (David *et al*, 2010).

Despite the implications of mutually exclusive splicing in organismal development and disease, current knowledge on the magnitude of MXE usage and its relevance in biological processes is far from complete. In order to obtain a genome-wide, unbiased estimate of the extent and biological role of mutually exclusive splicing in humans, a set of 6541 MXE candidates was compiled from annotated and novel predicted exons, and rigorously validated using over 15 billion reads from 515 RNA-seq datasets.

Results

The human genome contains 855 high-confidence MXEs

Compared to other splicing mechanisms, mutually exclusive splicing in humans seems to be a rare event. MXEs are characterised by genomic vicinity, splice site compatibility, and mutually exclusive presence in protein isoforms. Accordingly, the human genome annotation (GenBank v. 37.3) contains only 158 MXEs in 79 protein-coding genes (Supplementary Figs. S1 to S3). MXEs are often phrased ‘homologous exons’ in the literature because they likely originated from the same ancestral exon. We refrain from using this term throughout our analysis, because several MXEs present in the genome annotation do not show any sequence

homology and many neighbouring exons with high sequence similarity are not spliced in a mutually exclusive manner.

In a first attempt to chart an atlas of genome-wide mutually exclusive splicing in humans, we decided to predict potential MXE candidates and validate those using published RNA-seq data. In a first step, we generated a set of MXE candidates in the human genome (v. 37.3) from all annotated protein-coding exons and from novel exons predicted in intronic regions including only internal exons in the candidate list (Fig. 1A, Supplementary Figs. S1 to S4). From the annotated exons we selected those that appeared mutually exclusive in transcripts, and neighbouring exons that show sequence similarity and are translated in the same reading frame. To generate novel exon candidates we predicted exonic regions in neighbouring introns of annotated exons based on sequence similarity and similar lengths (Pillmann *et al*, 2011). We did not consider potential MXEs containing in-frame stop codons such as the neonatal-specific MXE reported for the sodium channel *SCN8A* (Zubović *et al*, 2012), and exons overlapping annotated terminal exons (Supplementary Fig. S2). The reconstruction resulted in a set of 6541 MXE candidates in 1542 protein-coding genes, including 1058 (68.6%) genes for which we predicted 1722 completely novel exons in previously intronic regions (Fig. 1B). Most introns in human genes are extremely long necessitating careful and strict validation of the MXE candidates to exclude false positive predictions (Lee & Rio, 2015).

To validate the predicted MXE candidates we made use of over 15 billion publically available RNA-seq reads, selecting 515 samples comprising 31 tissues and organs, 12 cell lines, and 7 developmental stages (Barbosa-Morais *et al*, 2012; Tilgner *et al*, 2012; Djebali *et al*, 2012; Yan *et al*, 2013; Xue *et al*, 2013; Fagerberg *et al*, 2014) (Supplementary Table S1). The data were chosen to encompass common and rare potential splice events in a broad range of tissues, cell types, and embryonic stages. Accordingly, the transcription of 6466 (99%) of

the MXE candidates is supported by RNA-seq reads mapped to the genome (Supplementary Fig. S3A). To be validated as true mutually exclusive splicing event, each MXE of a cluster needed to exhibit splice junction (SJ) reads from every MXE to up- or downstream gene regions bridging the other MXE(s) of the cluster (Fig. 1A). In addition, MXEs should not exhibit any SJ reads to another MXE except when the combined inclusion causes a frameshift and therefore a premature stop codon (Fig. 1A, Supplementary Figs. S3D, S5, and S6). These stringent criteria define a high-confidence set of MXEs, requiring three constraints for a cluster of two MXEs and already 18 constraints for a cluster of five MXEs (Supplementary Fig. S7). In case of clusters with more than two MXE candidates the validation criteria were applied to the cluster including all MXE candidates as well as to all possible sub-clusters to identify the largest cluster fulfilling all MXE criteria. According to these criteria, 1399 MXEs were verified with at least one SJ read per exon (1SJ), supported by 2.2 million exon mapping and 34 million SJ reads, increasing the total count of human MXEs by almost an order of magnitude (158 to 1399) (Fig. 1B, Supplementary Table S2). 855 MXEs were found to be supported by at least 3 splice junction reads per exon (3SJ) validated by 1.5 million exon mapping and 27 million SJ reads (Supplementary Figs. S8 to S10). The 1399 (855, numbers in brackets refer to the 3SJ validation) verified MXEs include 122 (112) annotated MXEs (Fig. 1B ‘annotated MXE’), 623 (388) exons that were previously annotated as constitutive or differentially included (‘annotated other splicing’), and 654 (358) exons newly predicted in intronic regions (‘novel exon’). Our analysis also showed that 29 of the 158 annotated MXEs are in fact not mutually exclusively spliced but represent constitutively spliced exons or other types of alternative splicing (Supplementary Fig. S2). Finally, 1741 (2336) MXE candidates including 1090 (1402) newly predicted exons and 17 (29) of the annotated MXEs are supported by 0.5 million exon and 13 million SJ matching reads but still have to be regarded

as MXE candidates because not all annotation criteria were fulfilled (Supplementary Figs. 3A and 3E).

To estimate the dependence of MXE confirmation and rejection on data quantity we cross-validated the MXE gain (validation) and loss (rejection) events for several subsets of the total RNA-seq data (Fig. 1C and Supplementary Fig. S11). The course of the curves provides strong evidence for the validity of the MXEs because a single exon-joining read would already be sufficient to reject an MXE cluster while at least two SJ reads are needed to validate one. Whereas even 15 billion RNA-seq reads do not achieve saturation for the amount of validated MXEs, the gain in rejected MXE candidates is virtually saturated using 25% of the data. In summary, the high-confidence set of 1399 (855) MXEs extends current knowledge of human MXE usage by an order of magnitude, (re)-annotating over a thousand existing and predicted exons and isoforms, while suggesting the existence of further human MXEs.

The human genome contains large cluster and multi-cluster MXEs

In general, mutually exclusive splicing can be quite complex. This is best demonstrated by genes in arthropods that contain both multiple MXE clusters ('multi-cluster') and large clusters with up to 53 MXEs such as in the *Drosophila Dscam* genes (Graveley *et al*, 2004; Pillmann *et al*, 2011). This is in strong contrast to mutually exclusive splicing in vertebrates as there is to date no evidence of multi-cluster or higher order MXE clusters (Matlin *et al*, 2005; Wang *et al*, 2008; Pan *et al*, 2008; Gerstein *et al*, 2014; Abascal *et al*, 2015a, 2015b).

The analysis of the 1399 validated human MXEs provides first evidence for clusters of multiple MXEs in the human genome (Fig. 1D, Supplementary Fig. S12). While most MXEs are present in clusters of two exons (1116 MXEs) a surprisingly high number of clusters have three to ten MXEs (283 MXEs in 71 clusters).

Interestingly, although a large part of the verified MXEs contain a single MXE cluster (554 genes, Fig. 1E) we could also provide evidence for human genes containing multiple MXE clusters. Thus, *TCF3*, *NEB*, *ANKRD36C*, and *MTHFD1L* contain three clusters, and *TTN*, *CAMK2D*, and *CUX1* four clusters of MXEs. A very interesting case of complex interleaved mutually exclusive splicing can be seen for *CUX1*, the transcription factor Cut-like homebox 1. It contains a cluster of MXEs (exons 3b - 3e) that is differentially included into a set of two exons (exon 3 and exon 4), and the two sets are themselves mutually exclusive (Fig. 1F, Supplementary Figs. S13 and S14). The identification of large clusters with multiple MXEs and many genes with multiple clusters shows that complex mutually exclusive splicing is not restricted to arthropods (Schmucker *et al*, 2000; Graveley, 2005; Lee *et al*, 2010; Hatje & Kollmar, 2013) but might be present in all bilateria.

Mutually exclusive splicing is tightly regulated at the RNA and protein level

To gain mechanistic insights into the regulation of mutually exclusive splicing in humans we investigated four mechanisms that were shown to act in some specific cases and were proposed to coordinate mutually exclusive splicing in general (Fig. 2A) (Letunic *et al*, 2002; Smith, 2005). We identified six cases (0.95%) of U2 and U12 splice acceptor incompatibility (Supplementary Fig. S15), 57 cases of a too short distance between splice donor sites and branch points (< 50 bp), and 377 (60%) cases of frame-shift that would result in non-functional mRNAs in case of combined inclusion (Supplementary Figs. S16 and S17). MXE-joining reads were found for 83 (22%) of these MXE clusters, 91 (75%) of the annotated and 25 (4%) of the predicted MXEs, suggesting that splicing of the remaining MXE clusters is tightly regulated by other mechanisms (Fig. 2B, Supplementary Figs. S3A, S3D) such as RNA-protein interactions, interactions between small nuclear ribonucleoproteins and splicing

factors (Lee & Rio, 2015), and competitive RNA secondary structural elements (Graveley, 2005; Yang *et al*, 2012; Suyama, 2013; Lee & Rio, 2015) (Supplementary Fig. S18).

In contrast to cassette exons and micro-exons, which tend to be located in surface loops and intrinsically disordered regions instead of folded domains (Buljan *et al*, 2012; Ellis *et al*, 2012; Irimia *et al*, 2014), all MXEs, whose structures have been analysed, are embedded within folded structural domains as has been shown for e.g. *DSCAM* (Meijers *et al*, 2007), *H2AFY* (Abascal *et al*, 2015a), the myosin motor domain (Kollmar & Hatje, 2014), and *SLC25A3* (Tress *et al*, 2016). As we have shown in the beginning and have shown for *Drosophila* (Hatje & Kollmar, 2013), there is also a subset - of unknown size - of MXEs not showing any sequence homology. If the exons of this subset were true MXEs and not mis-classified because of so far missing exon-joining reads, it would seem unlikely that the encoded peptides are part of the same folded domains. Here, we focused on exons with similar length and sequence similarity. Because of this similarity we assumed that MXEs modulate protein functions through variations in specific restricted parts of the structure as has been pointed out before (Tress *et al*, 2016). We identified three parameters that distinguish MXEs and cassette exons at a structural level. The defining feature of a cassette exon is that it can either be present or absent in the transcript. Thus, A) if one or both ends of the MXE-encoded peptide end within a secondary structural element it seems impossible that this exon could be absent from the transcript (=> cassette exon) because this would break up multiple spatial interactions. B) High sequence similarity between MXEs suggests important conserved structural interactions even if the peptide ends are not part of secondary structural elements. C) If the MXE-encoded peptide ends are far apart it seems extremely unlikely that the respective domain can fold correctly if the peptide is absent (=> cassette exon) and the open ends are joined. To assess this model, MXEs were mapped against the PDB database (Fig. 2C) (Rose *et al*, 2015). In 87% of the 543 MXEs matched to human or mammalian

protein structures at least one of the exon termini is embedded within a secondary structural element, supporting the hypothesis that MXEs modulate but do not considerably alter protein functions (Letunic *et al*, 2002; Yura *et al*, 2006; Abascal *et al*, 2015a; Tress *et al*, 2016) (Supplementary Fig. S19, Supplementary Table S3). Of the remaining 13% (blue colour in Fig. 2C), many MXEs would lead to frame shifts if they were cassette exons (blue circles), and in multiple cases (e.g. *COL9A3*, *COL24A1*, and *COL13A1*) the peptide ends are far apart indicating strong folding problems in case the respective exons were absent in the transcripts. In total, there are only a handful cases such as the MXE cluster in *ARL15* (Fig. 2C) whose mutually exclusive presence in proteins cannot be explained by the analysed splicing restrictions, by NMD-targeting, or by folding constraints.

MXEs mainly consist of one ubiquitous exon and otherwise regulated exons

To modulate gene functionality, mutually exclusive splicing would need spatial and temporal splicing regulation and expression (Wang *et al*, 2008; Tress *et al*, 2016). To understand the expression patterns of MXEs we conducted a differential inclusion analysis using the Human Protein Atlas (Fagerberg *et al*, 2014), Embryonic Development (Yan *et al*, 2013), and ENCODE datasets (Djebali *et al*, 2012). Of the 1399 MXEs, 299 MXEs (224 unique genes), 325 MXEs (234 unique genes), and 714 MXEs (432 unique genes) are differentially expressed, respectively (adjusted P-value < 0.05; Fig. 3A; Supplementary Figs. S20 to S23; Additional files 3 and 5). Most notably, the differentially expressed MXEs comprise 22.5%, 28.9% and 53.9% of all MXEs indicating that MXEs are to a very large extent tissue- and developmental stage-specifically expressed.

The comparison of the genes containing differentially expressed MXEs from these three projects shows that 499 (85.3%) of all 585 MXE cluster containing genes have at least a single MXE differentially expressed in one of the covered tissues, cell-types or developmental

stages (Fig. 3B). The 499 genes contain 914 differentially expressed MXEs (65% of the total 1399 MXEs; Fig. 3C). This number is in agreement with earlier analyses on small sets of MXEs (66% and 57%) (Wang *et al*, 2008; Abascal *et al*, 2015a), highlighting that MXE expression might be considerably more tissue-specific than the expression of other alternatively spliced exons. Interestingly, 116 MXEs from 36 genes are preferentially expressed during embryonic development indicating that many MXEs are specific to certain developmental stages (Figs. 3B and 3C).

The analysis of MXE specificity reveals that in many clusters one MXE dominates expression whereas other MXEs are expressed at selected developmental time-points and in specific tissues (Fig. 3, Supplementary Figs. S20 to S23). This modulation suggests crucial spatio-temporal functional roles for MXEs and can in many cases not be observed at the gene-level, as gene counts can remain largely invariant. A well-known case for similar expression of MXEs in newborn heart but expression of only one MXE variant in adult heart is the ion channel *CACNA1C* (Diebold *et al*, 1992), an example for the switch of expression are the MXEs of the *SLC25A3* gene (Wang *et al*, 2008). We surmise that the observed specificity in combination with a generally lower expression could also explain the discovery of 654 (358) novel exons that have so far eluded annotation efforts (Fig. 1A, Supplementary Fig. S20). In conclusion, the tight developmental and tissue-specific regulation of MXE expression suggests that changes in MXE function or expression might cause aberrant development and human disease (Xiong *et al*, 2015). Pathogenic mutations in MXEs are known to cause Timothy syndrome, cardiomyopathy, cancer, and kidney disease (Splawski *et al*, 2004, 2005; Mayr *et al*, 2011; David *et al*, 2010; Kaplan *et al*, 2000).

MXEs are high-susceptibility loci for pathogenic mutations

To obtain a comprehensive overview of MXE-mediated diseases we annotated all MXEs with

pathogenic SNPs from ClinVar (Landrum *et al*, 2016), resulting in 35 MXEs (eight newly predicted exons) with 82 pathogenic SNPs (Fig. 4, Supplementary Table S5). Disease-associated MXEs show tight developmental and tissue-specific expression (average Gini-index of 0.65) with prominent selective expression in heart and brain, and cancer cell lines (Fig. 4C, Supplementary Table S4). Interestingly, the percentage of genes with MXEs, which carry pathogenic SNPs, of all genes with MXEs is two-fold higher than the percentage of pathogenic SNP-carrying genes of all other genes. The genes with MXEs carrying pathogenic SNPs are predominantly associated with neurological disease (10), neuromuscular disorders (7), cardiomyopathies (6), and cancer (3), and are enriched in voltage-gated cation channels (e.g. *CACNA1C-D*), muscle contractile fiber genes (e.g. *TPM1*), and transmembrane receptors (e.g *FGFR1-3*) (Fig. 4, Supplementary Fig. S24, Supplementary Table S5).

Disease-associated MXEs have high amino-acid identity (average 49.1%, SD 23.1%), reaching up to 89% in *ACTN4*, suggesting similar functional roles and in consequence similar pathogenic potential for many MXE pairs (Fig. 4C, Supplementary Fig. S25). It is therefore surprising that only four of all SNP-containing MXE clusters contain mutations in both MXEs (*FHL1*, *MAPT*, *CACNA1C and CACNA1D*), whereas 31 currently have pathogenic SNPs in only one MXE. The MXE expression analysis shows that many SNP-carrying MXEs are highly expressed, especially in disease-associated tissues where the respective non-SNP-carrying MXEs are not or barely expressed (Fig. 4B-C, Supplementary Fig. S26). Examples include *ACTN4*, *TPM1*, and *SCL25A3* (Supplementary Figs. S25, S27, and S28). Moreover, MXEs with pathogenic SNPs are usually not or non-exclusively expressed at early developmental stages (Fig. 4C, Supplementary Fig. S30), while high and exclusive expression could lead to early embryonic death or severe multi-organ phenotypes (e.g. *FAR1*, Supplementary Figs. S29). Conversely, several non-SNP-carrying MXEs are highly expressed in early development, and are otherwise mainly expressed at equal and lower levels compared

to the SNP-carrying MXEs (Supplementary Figs. S27 and S28). The absence of pathogenic SNPs in these MXEs suggests functional compensation of the pathogenic SNP-carrying MXEs or early lethality, both of which would result in no observable phenotype.

Of the 35 MXE clusters with pathogenic mutations eight contain novel exons (Fig. 4C, Supplementary Table S6). A mutation in exon 9a (p.Asp365Gly) of *FAR1*, a gene of the plasmalogen-biosynthesis pathway, causes Rhizomelic chondrodysplasia punctata (RCDP), a disease that is characterized by severe intellectual disability with cataracts, epilepsy, and growth retardation (Buchert *et al*, 2014). Novel MXE 9b is expressed in the same tissues but at 8-fold lower levels suggesting partial functional compensation of the MXE 9a mutation, which might be responsible for the 'milder' form of RCDP as compared to pathogenic mutations in other genes of the pathway (*PEX7, GNPAT,* and *AGPS*) (Supplementary Fig. S29). A tissue-specific compensation mechanism had already been proposed but a reasonable explanation could not be given because *FAR2* expression shows a different tissue profile and individuals with deficits in peroxisomal β-oxidation, a potential alternative supply for fatty alcohols, have normal plasmalogen levels (Buchert *et al*, 2014). Because of the young age of the affected children it is not known yet, whether a mutation in constitutive exon 4 (p.Glu165_Pro169delinsAsp), which could not be compensated in a similar way as the exon 9a mutation, leads to a strong RCDP-like phenotype (no survival of the first decade of life) or to a milder form such as the one caused by the exon 9a mutation.

In conclusion, it is tempting to speculate that MXE pathogenicity might be governed by high or exclusive expression in affected target tissues that is usually absent from early developmental processes, a pattern of expression that seems at least partially inversed for MXEs without pathogenic SNP annotations. To assess whether MXE pathogenicity follows observable rules we trained a machine learner on MXE expression data and predicted the affected target tissue (Fig. 4D, Supplementary Table S6). To obtain at least ten observations

per category with an expression > 3 RPKM, diseases were grouped into cardio-neuromuscular (n=10) and other diseases (n=14) and predicted using leave-one-out cross-validation with a Random Forest. Cardiac-neuromuscular diseases could be predicted with an accuracy of 79% (p-value = 0.03), a specificity of 71%, a sensitivity of 90% and an area under the ROC curve (AUC) of 79% (Fig. 4D, Supplementary Table S6). Although based on only 24 observations, our data suggests that MXE expression might predict disease pathogenicity in space and potentially also in time.

Rapid gain and loss of MXEs in mammalian evolution

While tissue-specific gene expression is conserved between birds and mammals, the alternative splicing of differential inclusion exons is conserved only in brain, heart and muscles and is mainly lineage-specific (Merkin *et al*, 2012; Barbosa-Morais *et al*, 2012). Accordingly, a core of only ~500 exons was identified with conserved alternative splicing in mammals and high sequence conservation. In contrast, most of the known human MXEs have been shown to be highly conserved throughout mammals if not even vertebrates (Letunic *et al*, 2002; Copley, 2004; Abascal *et al*, 2015b). In order to assess the conservation of human MXEs across mammals we identified orthologous proteins in 18 representative species from all major sub-branches spanning 180 million years of evolution and predicted MXEs therein (Fig. 5, Supplementary Fig. S30, Supplementary Table S7). Based on a simple model expecting each shared cluster to be already present in the last common ancestor of the respective species, the evolution of the MXE clusters is characterised by a core set of at least 173 (28%) of the human MXE clusters conserved throughout mammals (Fig. 5, Supplementary Fig. S30). These MXE clusters include 83 clusters shared between at least 16 of the species and 61 clusters shared between 17 species while the other MXEs are subject to branch- and species-specific cluster gain and loss events. The clusters absent in specific

branches most likely do not represent cases of missing data but taxon-specific loss events, such as the MXE clusters in the *SRPK1* and *PQBP1* genes, which are absent in Glires (including mouse and pika), the cluster of ten MXEs in *ABI3BP* that has been lost in the ancestor of mouse and rat, the MXEs in *OSTF1* and *PTPRS*, which are absent in Afrotheria, and the MXE clusters in *IKZF3*, *MBD1* and *ATP10B*, which are present in all Eutheria (16 species, placental mammals) but not in Metatheria (marsupials). The MXE cluster gain rate within eutherian evolution towards human is relatively constant over time with about 23 clusters per 10 million years. Interestingly, the 16 eutherian species lost similar numbers of MXE clusters compared to human (127 clusters on average, Supplementary Fig. S30). Although the overlap of MXEs in orthologous genes of human and *Drosophila* is very low and their presence has been attributed to convergent evolution (Copley, 2004), the MXE gain and loss rates are very similar (Hatje & Kollmar, 2013) indicating a conserved role of tandem exon duplication in bilaterians. Gene structures can be highly conserved between kingdoms (Rogozin *et al*, 2003) and certain exons therefore seem to be predisposed to undergo duplication. In summary, these findings provide strong evidence for many MXE gain and loss events during mammalian evolution, suggesting a pronounced role of these processes in speciation and establishing phenotypic differences.

Discussion

Using stringent criteria, including sequence similarity, reading frame conservation and similar lengths, and billions of RNA-seq reads we generated a strongly validated atlas of 1399 human MXEs providing insights into mutually exclusive splicing mechanics, specific expression patterns, susceptibility for pathogenic mutations, and deep evolutionary conservation across 18 mammals. The presented increase of human MXEs by an order of magnitude lifts MXEs into the present-day dimension of other human alternative splice types (Wang *et al*, 2008; Pan

et al, 2008; Gerstein *et al*, 2014). Saturation analysis and the existence of 1816 expressed but unconfirmed MXE candidates promise a potential two-fold increase of the MXE-ome with further sequence data incorporated. Although alternative splice variants are abundant at the transcriptome level, recent mass spectrometry analyses suggested only small numbers of alternative transcripts to be translated (Ezkurdia *et al*, 2015; Abascal *et al*, 2015a). Interestingly, MXEs were particularly enriched in the translated alternative transcripts, compared to other splice variants. However, ribosome profiling data showed high frequencies of ribosome engagement of cassette exons indicating that these isoforms are likely translated (Weatheritt *et al*, 2016). Similar results have been obtained through polyribosome profiling (Sterne-Weiler *et al*, 2013; Floor & Doudna, 2016). These observations suggest that most of the MXEs evaluated at the transcript level will also be found in the proteome.

About half (47%) of the 1399 MXEs represent novel exons, which are often expressed at low levels and whose expression is restricted to few tissues and cell-types, possibly explaining their absence from current genome annotations. Extrapolating these observations to all splice types and genes suggests the existence of thousands yet unannotated exons in introns. This estimation is in accordance with a recent analysis of more than 20000 human RNA-seq datasets that revealed over 55000 junctions not present in annotations (Nellore *et al*, 2016). In this analysis, junctions found in at least 20 reads across all samples were termed 'confidently called'. Although the total number of reads required for MXE validation in our analysis is lower ($\geq$ 2 SJ reads in the 1SJ case, $\geq$ 6 SJ reads in the 3SJ case), the numbers seem more conservative given that we used 40 times less datasets for the validation.

The almost ten-fold increase in the human MXE-ome supports recent suggestions that mutually exclusive splicing might play a much more frequent role than anticipated (Wang *et al*, 2008; Pan *et al*, 2008; Ezkurdia *et al*, 2012; Abascal *et al*, 2015a). By comparing

differentially expressed MXEs across cell-types, tissue-types, and development we could show that 14% of all genes with MXE clusters are shared between the three data sources, and 39% between any two. Most notably, however, it is almost always a different MXE from the same cluster that is differentially expressed, and only 3.3% of the MXEs are differentially expressed in all three data sources. We believe that this indicates a high spatio-temporal regulation of all MXEs in two-exon and multi-exon clusters. We rarely observed switch-like expression with only one of the MXEs of each cluster present in each cell- or tissue-type or developmental stage. Rather, one of the MXEs ('default MXE') of each cluster was present in most or all samples and the other MXEs were expressed in several selected tissues and developmental stages ('regulated MXEs') in addition to the default MXE. Although the 'regulated MXE' is usually expressed at lower level compared to the 'default MXE', there is almost always at least a single tissue or developmental stage where it is expressed at higher level. This supports previous assertions on the modulatory and compensatory effects of the regulated MXE on the enzymatic, structural or protein-interaction functions of the affected protein domains (Letunic *et al*, 2002; Tress *et al*, 2016).

The concerted annotation and splicing analysis of novel exons has deep implications for the detection and interpretation of human disease (Bamshad *et al*, 2011; Gonzaga-Jauregui *et al*, 2012; Xiong *et al*, 2015; Bowdin *et al*, 2016). For one, exome and panel sequencing remain the method of choice for the detection of genetic diseases and both methods rely on current exon annotations (Chong *et al*, 2015). Furthermore, our data suggest that MXE expression might reflect disease pathogenesis that could allow for the prediction of the affected organ(s). It is intriguing to speculate that the observed expression-disease association is a general dogma, which could be used to predict yet unseen diseases from published expression data, potentially bringing about a paradigmatic shift in (computational) disease research.

Materials and Methods

Data sources

The human genome assembly and annotated proteins (all isoforms) were obtained from GenBank (v. 37.3) (Benson *et al*, 2013). For MXE candidate validation, we selected data from 515 publically available samples comprising 31 tissues and organs, 12 cell lines, and 7 developmental stages (Barbosa-Morais *et al*, 2012; Tilgner *et al*, 2012; Djebali *et al*, 2012; Yan *et al*, 2013; Xue *et al*, 2013; Fagerberg *et al*, 2014) amounting to over 15 billion RNA-seq reads. The data were chosen to encompass common and rare potential splice events in a broad range of tissues, cell types, and embryonic stages. These RNA-seq data were obtained from either GEO (NCBI) or ENA (EBI) databases (Supplementary Table S1A). The description of the respective tissues and developmental stages is listed in Supplementary Table S1B.

Reconstruction of gene structures

The gene structures for the annotated proteins were reconstructed with Scipio (Keller *et al*, 2008; Hatje *et al*, 2013) using standard parameters except `--max_mismatch=7`, `--region_size=20000`, `--single_target_hits`, `--max_move_exon=10`, `--gap_to_close=0`, `--blat_oneoff=false`, `--blat_score=15`, `--blat_identity=54`, `--exhaust_align_size=20000`, and `--exhaust_gap_size=50`. We let Scipio start with `blat_tilesize=7` and, if the entire gene structure could not be reconstructed, reduced the `blat_tilesize` step by step to 4. All parameters are less stringent than default parameters to increase the chance to reconstruct all genes automatically.

Predicting mutually exclusive spliced exons

The human genome annotation does not contain specific attributes for alternative splice variants and thus does not allow extracting or obtaining lists for specific splice types. As mutually exclusive spliced exons (MXEs) we regarded those neighbouring exons of a gene locus that are present in only one of the annotated splice variants. These MXEs were termed "annotated MXEs". However, exons appearing mutually exclusive are not necessarily spliced as MXEs. Terminal exons for example are included in transcripts by alternative promoter usage and by alternative cleavage and polyadenylation. MXEs were predicted in the reconstructed genes using the algorithm implemented in WebScipio (Pillmann *et al*, 2011). The minimal exon length was set to 10 aa (`--min_exon_length=10`). WebScipio determines the length of each exon ("search exon") and generates a list of potential exonic regions with identical lengths (to preserve the reading frame) within the neighbouring up- and downstream introns. To account for potential insertions, we allowed length differences between search exon length and potential new exonic region of up to 60 nucleotides in steps of three nucleotides (`--length_difference=20` [given in aa]), thus obtaining a list of "exon candidates". WebScipio then translates all exon candidates in the same reading frame as the search exon and removes all sequences that contain an in-frame stop codon. In case of overlapping exonic candidate regions, we modified the original WebScipio algorithm to favour exonic regions with GT---AG splice junctions over other possible splice sites (GC---AG and GG---AG). The translations of the exon candidates are then compared to the translations of the search exons, and candidates with an amino-acid similarity score of more then ten (`--min_score=10`) are included in the final list of MXE candidates. Because the exon candidate scoring is done at the amino acid level, WebScipio expects candidates for 5' exons of genes to start with a methionine, and candidates for 3' exons of genes to end with a

stop codon. This minor limitation is due to WebScipio's original development as gene reconstruction software. MXE candidates for terminal exons were only searched in direction to the next/previous internal exon. The reason for looking for MXE candidates of annotated terminal exons is that we cannot exclude that further up- and downstream exons are missing in the annotation, which would turn the new MXE candidates to internal exons. Because of the described minor limitation, however, we can only propose MXE candidates if supposed additional up- and downstream exons are non-coding exons. Because terminal exons are included in transcripts by alternative promoter usage and by alternative cleavage and polyadenylation, we treated the list of terminal exon candidates separately (Supplementary Fig. S4). This list might be of interest for further investigation for other researchers. Except for this Supplementary Fig. S4, we entirely focused on internal MXE candidates.

Definition of criteria for RNA-seq evaluation of the MXE candidates

While the sole mapping of RNA-seq reads reveals the transcription of the respective genomic region it does not prove the inclusion into functional transcripts. The mutually exclusive inclusion of the MXE candidates into functional transcripts requires at least the following splice junction (SJ) reads (Supplementary Fig. S5): A) There must be SJ reads matching from every MXE to up- or downstream gene regions bridging the other MXEs of the cluster. The latter criterion takes into account that the annotated exons neighbouring the clusters of MXEs might not themselves be constitutive but alternative exons as for example in *NCX1* (Supplementary Fig. S6). B) SJ reads mapping from one to another MXE candidate lead to MXE candidate rejection except for those MXEs leading to a frame shift. Without this constraint, which has not been set in earlier analyses (Wang *et al*, 2008) MXEs cannot be distinguished from neighbouring differentially included exons, which are quite common in human (data not shown; see for example (Hammesfahr & Kollmar, 2012) and Supplementary

Fig. S6). Thus, there are three constraints for a cluster of two MXEs while clusters of three and five MXEs, for example, already require seven and 18 constraints, respectively (Supplementary Figs. S5 and S7). Under more stringent conditions, also SJ reads from MXEs to the neighbouring annotated exons independent of their splice type would be required giving rise to five constraints for a cluster of two MXEs (Supplementary Fig. S5).

Note that as a matter of principle the read coverage of every single MXE is considerably lower than that of constitutive exons due to their mutually exclusive inclusion in the transcripts. For example, each of the exons of a cluster of three MXEs is expected to only have, on average, one-third the coverage of the constitutive exons of the same gene. The number of predicted exons, of which both sites are supported by splice junction reads, is also considerably lower than the total number of supported MXE candidates (Supplementary Fig. S3), which we think is due to the general low coverage of the exons and not due to read mapping and exon border prediction problems (Supplementary Fig. S3).

Validation of the MXE candidates by RNA-seq mapping

SRA files were converted to FASTQ files using fastq-dump software (v. 2.1.18). FASTQ files were mapped onto the human reference genome (hg19) using the STAR aligner (v_2.3.0e_r291) (Dobin *et al*, 2013). To this end, we first generated a reference genome index with `--sjdbGTFfeatureExon`, `--sjdbGTFtagExonParentTranscript`, a splice-junction overhang size of 99 (`--sjdbOverhang`) and GTF annotation files containing all transcripts and all MXE candidates. The MXE candidate GTF file was extracted from Kassiopeia database and is available for download there (Hatje & Kollmar, 2014). The mapping was done for each sample separately. We allowed a rather stringent maximum mismatch of 2 (`--outFilterMismatchNmax 2`; STAR default is 10) and the output was forced to SAM format (`--outStd SAM`). Otherwise, default settings were used. The

resulting files with the mapped reads were sorted, converted to BAM format and indexed with SAMtools (`sort -n`) for further processing (Li *et al*, 2009).

Distinguishing MXEs from other splice variants

For the analysis of the read mapping data we disassembled clusters with more than two MXE candidates into all possible sub-clusters. E.g. a cluster with four MXE candidates [1,2,3,4] was fractionated into the following sub-cluster: [1,2], [2,3], [3,4], [1,2,3], [2,3,4], [1,2,3,4]. Each of these sub-clusters was analysed independently according to the validation criteria (splice junction reads present, exon joining reads absent). If all criteria were satisfied for one of the sub-clusters, all MXE candidates of the respective sub-cluster were labelled “verified”. In a second analysis, each cluster of MXE candidates was analysed for exon joining reads, which denote constitutive splicing or splicing as differentially included exons. However, MXE candidates of clusters and sub-clusters with exon joining reads but exon lengths not divisible by three were also flagged as “verified” because their combined inclusion would lead to a frame-shift in the translation of the transcript.

Limits of the MXE dataset

Similar to every genome annotation dataset, also the current dataset of RNA-seq validated MXEs has some limitations. Some are inherent to the still incomplete human genome annotation that was used as basis for generating the list of MXE candidates. As mentioned above and shown in Supplementary Fig. S2C, there are genes with mis-annotated terminal exons overlapping MXEs. Also, there are “transcripts” in the GenBank dataset that combine exons from (now) different genes. The presence of these “transcripts” in the genome annotation might be the result of mis-interpreting cDNA data as coding sequence although these might be the result of some level of mis-splicing.

Similarly, mis-splicing might be an important reason for validating true MXEs as "non-MXEs". A single exon-joining read turns MXE candidates into non-MXEs, whose mutually exclusive splicing might otherwise be supported by thousands of MXE-bridging SJ reads. Given these limitations we expect that many of the exons, that we currently tag as constitutive or other alternative splicing, might in fact be MXEs. On the other hand, our MXE dataset might also contain some exons, that are in fact non-MXEs. This is well demonstrated in the saturation analysis (Fig. 1C) showing that although more data will lead to the validation of many more exons as MXEs, for which SJ reads are currently missing, there will be clusters that will be rejected as soon as more data include exon-joining reads. In addition, some MXEs with only a few supporting SJ reads might in fact be pseudoexons. However, we also did not observe any SJ reads for about 15% of the annotated exons, which are nevertheless not regarded as pseudoexons (Fig. 1B, Supplementary Fig. S3). Finally, some MXEs determined from transcripts showing complex splicing might in fact be mutually exclusive in transcripts, but not in the sense of a cluster of uninterrupted neighboring exons.

Saturation Analysis

Sub-samples of STAR-aligned RNA-seq splice junction (SJ) reads were used to estimate the expected recall and false positive rate. The number of verified MXEs was calculated using SJ reads for different percentages of the data. To reduce the bias from data sampling, datasets were chosen randomly and the saturation analysis was performed in 30 independent runs. To calculate the mean of validated and rejected MXEs at respective percentages of the total RNA-seq data used for validation, we used the respective numbers from the 30 independent runs.

Analysis of the splice mechanism

To determine the distance between intron donor site and branch point we analysed all introns smaller than 500 bp using the standalone version of SVM-BPfinder (beta) (Corvelo *et al*, 2010) to predict branch point locations. Longer introns harbour high numbers of branch point candidates and the accuracy of the branch point prediction considerably decreases. Longer introns also often contain multiple branch points with different splicing kinetics (Corvelo *et al*, 2010) so that a steric hindrance criterion for splicing multiple MXEs into the same transcript might not apply anymore. Branch points are usually located in the 3' regions of the introns and it seems highly unlikely to identify only a single potential branch point within an e.g. >2000 bp intron, which would in addition be located within the 5' 50 bps. Thus, the highest-scoring location within the <500 bp introns was taken as best guess for the branch point and the distance to the intron donor site determined.

In order to identify U12-type introns we analysed all donor splice sites of the introns preceding the clusters of MXEs and those subsequent to all MXEs using the consensus pattern described by Sharp and Burge (Sharp & Burge, 1997). The acceptor splice sites of U12-type introns do not show conserved patterns and were therefore not used here for verification.

Binding windows for competing intron RNA secondary structures were predicted for all candidate clusters of MXEs using the SeqAn package (Döring *et al*, 2008). The identified binding windows of all homologous genes were aligned using MUSCLE (Edgar, 2004) and the RNA secondary structures predicted by RNAalifold (ViennaRNA package) (Lorenz *et al*, 2011).

Mapping MXE sequences onto protein structures

To identify the best structural models for the sequences encoded by the MXEs we mapped the protein sequences of the respective genes against available protein structure data. To this end,

we made use of a recently developed database, called Allora (`http://allora.motorprotein.de`), in which genomic information is mapped onto protein structures. Allora currently contains 94,148 PDB entries (derived from the RCSB Protein Data Bank, `http://www.rcsb.org`, (Rose *et al*, 2015)) with 247,959 chains, of which 120,665 represent unique sequences. Based on the database references in the PDB entries, the full-length proteins were fetched from UniProt KB (UniProt Consortium, 2015) or GenBank (Benson *et al*, 2013) and the corresponding gene structures of the eukaryotic proteins reconstructed with WebScipio (Hatje *et al*, 2013). In Allora, all PDBs belonging to the same UniProt or GenBank entries are connected. BLAST+ (Camacho *et al*, 2009) was used to search for the most similar UniProt/GenBank protein sequence compared to the human proteins containing MXEs. The hit with the lowest E-value was taken and the associated PDB chains were aligned to the human protein using m-coffee (Wallace *et al*, 2006). The MXE part of the alignment was extracted for further analysis (=> "MXE structure"). As "intron distances" we determined the distances between the CA-atoms of the first and the last residues of the MXE-structures.

Evaluating the differential inclusion of MXEs into transcripts

Read counts for both genes and exons were extracted using HTSeq-count v. 0.6.1 (Anders *et al*, 2015) with option `-m intersection-nonempty` and DEXSeq v. 1.12.2 (Anders *et al*, 2012) with options `--minaqual=10` and `--order=name` set for all samples, and options `--paired=yes` and `--paired=no` set depending on the input samples, respectively. DEXSeq was run on each of the six sequencing projects (Supplementary) separately. In case of the Illumina Human BodyMap Project, the experimental setup (single-end vs. paired-end reads) might dominate read counting and we therefore excluded the 16 paired-end read datasets from this project from the differential exon inclusion analysis. For

each project we created a DEXSeq input configuration file according to the software specifications with sample name, path to the count files, experimental conditions, and replicate numbers. In the condition column, we specified the tissue, cell type or embryonic developmental stage of each sample. Samples from the same condition are internally grouped together by DEXSeq as replicates. For main DEXSeq processing we used the input data as defined in the configuration files, extracted all exon counts and normalized the data to account for different sequencing coverage (`estimateSizeFactors` function). Based on the exon counts and the normalization (size factors) we computed the differential expressed exons (`testForDEU` function) and determined the respective relative exon usage fold changes (`estimateExonFoldChanges` function). The results were combined and stored in a CSV format file for further processing.

Differential expression of pairs of annotated and novel MXEs

For each sample (tissue, cell type, and developmental stage) we calculated the median RPKM (Reads Per Kilobase of transcript per Million mapped reads) from the replicates for each MXE. To compile a set of MXEs with significant expression, only pairs of MXEs were selected of which either the annotated or the novel exon had a median expression of more than 3. The number of MXEs for this analysis would not considerably decrease if a cut-off of 30 were chosen (245 MXEs at a cut-off of 3 versus 233 MXEs at a cut-off of 30). For each pair of MXEs we subtracted the expression value of the specific/novel/SNP-containing MXE from the expression of the respective ubiquitous/known/non-SNP-containing MXE and scaled those values between -1 (high expression ubiquitous/known/non-SNP-containing MXE) and 1 (high expression specific/novel/SNP-containing MXE) (see also Fig. 3a, Supplementary Fig. S20, and Fig. 4c). In case an MXE pair was not expressed in a certain tissues (NA or 0) the value was set to 0.

Inequality analysis

The mean RPKM values of each MXE were calculated for each tissue in the Human Protein Atlas project, each developmental stage in the embryonic development (Peking University) project, and each cell type in the ENCODE (Caltech) project. For each project, only MXEs with a mean RPKM ≥ 10 in at least one dataset were kept (978, 590, and 894 MXEs, respectively). For each MXE the Gini index (Ceriani & Verme, 2012) was calculated independently for each project based on the mean RPKM values using the Gini function with standard parameters from the ineq R package version 0.2-13 (Achim Zeileis, Christian Kleiber, `https://CRAN.R-project.org/package=ineq`) (Cowell, 2011). For the analysis of MXE clusters only those clusters were taken into account that include at least two MXEs with an RPKM ≥ 10 in at least one dataset within each project (318, 120, and 273 clusters, respectively).

Identification of pathogenic SNPs in MXEs

In order to identify potentially pathogenic SNPs in MXEs, the MXEs were compared to the ClinVar SNP database (ClinVar VCF file downloaded on 11 Aug 2016, version updated at 30 Jun 2016, (Landrum *et al*, 2016)). The ClinVar variant summary file (VCF file) was converted into a BED file keeping all original information. Positions overlapping between MXEs and ClinVar SNPs were accessed using the BEDTools feature intersection software (Quinlan & Hall, 2010). SNPs are classified as pathogenic or non-pathogenic according to ClinVar's 'ClinicalSignificance' field annotation. All entries containing 'benign' and all structural variations were removed. All ClinVar-SNPs overlapping with MXEs were manually verified in order to keep only potentially pathogenic variations. To access the statistical significance of disease enrichment, a hypergeometric test was applied using all

genes represented in ClinVar as background (27261 genes) and the genes containing annotated pathogenic SNPs (2992).

Disease prediction using pathogenic SNPs in MXEs

In order to predict disease from MXE expression we first filtered for MXEs that had a minimal RPKM value of 3 and then subtracted the expression of the non-SNP-containing MXE from the SNP-containing MXE for all MXE pairs with mutations, across all developmental stages, tissues, and cell types (49 features per MXE pair). Expression values were subsequently scaled and centred and the MXE pairs were annotated to two disease classes, cardiomyopathy-neuromuscular disease (n=10) or other diseases (n=14). We re-grouped genes into these categories to obtain relatively balanced categories while keeping a minimum of 10 observations per category.

Classification with limited observations needs careful execution, as over-fitting (high-variance) and under-fitting (high-bias) are common problems. To avoid high-variance or bias several crucial steps were taken. First, we did not optimize hyper-parameters, using a Random Forest with 250 trees and a maximum tree depth of 16 (number of predictors / 3). Second, we used leave-one-out cross-validation to avoid sampling bias and model instability. Third, diseases were grouped into two categories of relatively even size (see above).

Models were built using the R packages caret (Kuhn, 2008) and randomForest and ROC curves were generated with ROCR (Sing *et al*, 2005).

Gene Ontology enrichment analysis

We used WebGestalt for Gene Ontology enrichment analyses (Wang *et al*, 2013). The lists of unique genes in gene symbol format were uploaded to WebGestalt and the GO Enrichment Analysis selected. The entire human genome annotation was set as background and 0.05 as

threshold for the p-value for the significance test using the default statistical method "hypergeometric".

Protein interaction analysis

The protein-protein interaction network was built by using GeneMANIA webservice (Warde-Farley *et al*, 2010). The list of unique genes containing a pathogen SNP was submitted to GeneMANIA's webservice and we downloaded the resulting network in SVG format and manually included disease and ontology information.

Assessing the dynamics of MXE annotations over time

MXEs might have already been annotated/described although not been included in the NCBI reference dataset. This might especially account for newer annotations based on the recently published ENCODE project data. Therefore, we obtained alternative protein sequence datasets from Aceview (Thierry-Mieg & Thierry-Mieg, 2006) and Ensembl (Yates *et al*, 2016). Further datasets like the VEGA and GENCODE annotations are continuously integrated into Ensembl and were therefore not considered separately. The Aceview database has been built in the year 2000 to represent comprehensive and non-redundant sequences of all public mRNA sequences. The human dataset has last been updated in November 2011, thus before the availability of the ENCODE data.

To assess the novelty of our MXE assignments with respect to the timely updates and changes of the human annotations we compared our data with that of Aceview and with the latest annotation from Ensembl (Fig. 5, Supplementary Fig. S1). As at the beginning of the project, only a few MXEs are annotated as such in other databases. Surprisingly, however, many of the previously annotated exons (independent of their splicing status) were removed from the latest Ensembl annotation, although our RNA-Seq mapping not only strongly

supports their inclusion into transcripts but also their splicing as MXEs. This shows that further collaborative efforts are needed to reveal a stable and persistent human gene annotation.

Ab inito exon prediction

Exon prediction by ab initio gene finding software is another means of generating a database of potential coding sequences. Ab initio exon prediction was done with AUGUSTUS (Stanke & Waack, 2003) using default parameters to find alternative splice forms and the feature set for *Homo sapiens*.

Identifying orthologous proteins in 18 mammals

Cross-species searches in 18 mammals (Supplementary Table S7) were done with WebScipio (Hatje *et al*, 2013) with same parameters as for gene reconstructions except `--min_identity=60`, `--max_mismatch=0` (allowing any number of mismatches), `--gap_to_close=10`, `--min_intron_length=35`, `--blat_tilesize=6`, and `--blat_oneoff=true`. MXE candidates in cross-species gene reconstructions were searched with `–length_difference=20`, `--min_score=15`, and `--min_exon_length=15`, for all exons in all introns but not in up- and downstream regions. Reasons for not detecting clusters of MXEs might be gene and MXE loss events, sequence divergence precluding ortholog identification, and assembly gaps. For determining the origin of a conserved MXE cluster we used a simple model expecting each shared cluster to be already present in the last common ancestor of the respective species. This approach is equivalent to inferring ancestral character states with Dollo parsimony (Farris, 1977).

Data availability

All generated data can be searched, filtered and browsed at Kassiopeia (`www.motorprotein.de/kassiopeia`; (Hatje & Kollmar, 2014)). The datasets supporting the conclusions of this article are also included within the article and its additional files.

Competing interests

The authors declare that they have no competing interests.

Authors' contributions

MK initiated the study and designed the analyses together with SB. KH and BH performed MXE predictions. KH integrated the human MXE data into the Kassiopeia database. KH implemented MXE candidate extraction and RNA-seq analysis with help from ROV and SB. KH and MK did the cluster distribution, splicing mechanism, and protein structure mapping analyses. KH, ROV, RR, OS, SB and MK performed the differential expression analysis. ROV, RR, and SB performed the SNP mapping and prediction analysis. The comparison of different human gene annotations was done by KH and DS. KH did the prediction of MXEs in other mammals, and their comparison together with MK. MK and SB wrote the manuscript. ROV, KH, and RR contributed to manuscript text and Supplementary Materials. All authors read and approved the final manuscript.

Acknowledgements

We would like to thank Daniel Sumner Magruder from the Bonn group for critical suggestions. In particular, we would like to thank André Ahrens from the Kollmar group for

his tremendous help in implementing the Allora database and performing the mapping of MXEs onto protein structures. The Kollmar group would like to thank Prof. Christian Griesinger for his continuous generous support. We would like to thank Robert P. Zinzen and Carla Margulies for critical reading of the manuscript.

References

Abascal F, Ezkurdia I, Rodriguez-Rivas J, Rodriguez JM, Pozo A del, Vázquez J, Valencia A & Tress ML (2015a) Alternatively Spliced Homologous Exons Have Ancient Origins and Are Highly Expressed at the Protein Level. *PLOS Comput Biol* **11:** e1004325

Abascal F, Tress ML & Valencia A (2015b) The evolutionary fate of alternatively spliced homologous exons after gene duplication. *Genome Biol. Evol.* **7:** 1392–1403

Anders S, Pyl PT & Huber W (2015) HTSeq--a Python framework to work with high-throughput sequencing data. *Bioinformatics* **31:** 166–169

Anders S, Reyes A & Huber W (2012) Detecting differential usage of exons from RNA-seq data. *Genome Res*. **22:** 2008–2017

Bamshad MJ, Ng SB, Bigham AW, Tabor HK, Emond MJ, Nickerson DA & Shendure J (2011) Exome sequencing as a tool for Mendelian disease gene discovery. *Nat. Rev. Genet.* **12:** 745–755

Barbosa-Morais NL, Irimia M, Pan Q, Xiong HY, Gueroussov S, Lee LJ, Slobodeniuc V, Kutter C, Watt S, Çolak R, Kim T, Misquitta-Ali CM, Wilson MD, Kim PM, Odom DT, Frey BJ & Blencowe BJ (2012) The Evolutionary Landscape of Alternative Splicing in Vertebrate Species. *Science* **338:** 1587–1593

Benson DA, Cavanaugh M, Clark K, Karsch-Mizrachi I, Lipman DJ, Ostell J & Sayers EW (2013) GenBank. *Nucleic Acids Res.* **41:** D36-42

Blencowe BJ (2006) Alternative splicing: new insights from global analyses. *Cell* **126:** 37–47

Bowdin S, Gilbert A, Bedoukian E, Carew C, Adam MP, Belmont J, Bernhardt B, Biesecker L, Bjornsson HT, Blitzer M, D'Alessandro LCA, Deardorff MA, Demmer L, Elliott A, Feldman GL, Glass IA, Herman G, Hindorff L, Hisama F, Hudgins L, et al (2016) Recommendations for the integration of genomics into clinical practice. *Genet. Med.* **18:** 1075–1084

Buchert R, Tawamie H, Smith C, Uebe S, Innes AM, Al Hallak B, Ekici AB, Sticht H, Schwarze B, Lamont RE, Parboosingh JS, Bernier FP & Abou Jamra R (2014) A peroxisomal disorder of severe intellectual disability, epilepsy, and cataracts due to fatty acyl-CoA reductase 1 deficiency. *Am. J. Hum. Genet.* **95:** 602–610

Buljan M, Chalancon G, Eustermann S, Wagner GP, Fuxreiter M, Bateman A & Babu MM (2012) Tissue-specific splicing of disordered segments that embed binding motifs rewires protein interaction networks. *Mol. Cell* **46:** 871–883

Camacho C, Coulouris G, Avagyan V, Ma N, Papadopoulos J, Bealer K & Madden TL (2009) BLAST+: architecture and applications. *BMC Bioinformatics* **10:** 421

Ceriani L & Verme P (2012) The origins of the Gini index: extracts from Variabilità e Mutabilità (1912) by Corrado Gini. *J. Econ. Inequal.* **10:** 421–443

Chong JX, Buckingham KJ, Jhangiani SN, Boehm C, Sobreira N, Smith JD, Harrell TM, McMillin MJ, Wiszniewski W, Gambin T, Coban Akdemir ZH, Doheny K, Scott AF, Avramopoulos D, Chakravarti A, Hoover-Fong J, Mathews D, Witmer PD, Ling H, Hetrick K, et al (2015) The Genetic Basis of Mendelian Phenotypes: Discoveries, Challenges, and Opportunities. *Am. J. Hum. Genet.* **97:** 199–215

Copley RR (2004) Evolutionary convergence of alternative splicing in ion channels. *Trends Genet.* **20:** 171–176

Corvelo A, Hallegger M, Smith CWJ & Eyras E (2010) Genome-wide association between branch point properties and alternative splicing. *PLoS Comput. Biol.* **6:** e1001016

Cowell F (2011) Measuring Inequality Oxford University Press

David CJ, Chen M, Assanah M, Canoll P & Manley JL (2010) HnRNP proteins controlled by c-Myc deregulate pyruvate kinase mRNA splicing in cancer. *Nature* **463:** 364–368

Diebold RJ, Koch WJ, Ellinor PT, Wang JJ, Muthuchamy M, Wieczorek DF & Schwartz A (1992) Mutually exclusive exon splicing of the cardiac calcium channel alpha 1 subunit gene generates developmentally regulated isoforms in the rat heart. *Proc. Natl. Acad. Sci. U. S. A.* **89:** 1497–1501

Djebali S, Davis CA, Merkel A, Dobin A, Lassmann T, Mortazavi A, Tanzer A, Lagarde J, Lin W, Schlesinger F, Xue C, Marinov GK, Khatun J, Williams BA, Zaleski C, Rozowsky J, Röder M, Kokocinski F, Abdelhamid RF, Alioto T, et al (2012) Landscape of transcription in human cells. *Nature* **489:** 101–108

Dobin A, Davis CA, Schlesinger F, Drenkow J, Zaleski C, Jha S, Batut P, Chaisson M & Gingeras TR (2013) STAR: ultrafast universal RNA-seq aligner. *Bioinformatics* **29:** 15–21

Döring A, Weese D, Rausch T & Reinert K (2008) SeqAn An efficient, generic C++ library for sequence analysis. *BMC Bioinformatics* **9:** 11

Edgar RC (2004) MUSCLE: a multiple sequence alignment method with reduced time and space complexity. *BMC Bioinformatics* **5:** 113

Ellis JD, Barrios-Rodiles M, Colak R, Irimia M, Kim T, Calarco JA, Wang X, Pan Q, O'Hanlon D, Kim PM, Wrana JL & Blencowe BJ (2012) Tissue-specific alternative splicing remodels protein-protein interaction networks. *Mol. Cell* **46:** 884–892

Ezkurdia I, Pozo A del, Frankish A, Rodriguez JM, Harrow J, Ashman K, Valencia A & Tress ML (2012) Comparative Proteomics Reveals a Significant Bias Toward Alternative Protein Isoforms with Conserved Structure and Function. *Mol. Biol. Evol.* **29:** 2265–2283

Ezkurdia I, Rodriguez JM, Carrillo-de Santa Pau E, Vázquez J, Valencia A & Tress ML (2015) Most highly expressed protein-coding genes have a single dominant isoform. *J. Proteome Res.* **14:** 1880–1887

Fagerberg L, Hallström BM, Oksvold P, Kampf C, Djureinovic D, Odeberg J, Habuka M, Tahmasebpoor S, Danielsson A, Edlund K, Asplund A, Sjöstedt E, Lundberg E, Szigyarto CA-K, Skogs M, Takanen JO, Berling H, Tegel H, Mulder J, Nilsson P, et al (2014) Analysis of the human tissue-specific expression by genome-wide integration of transcriptomics and antibody-based proteomics. *Mol. Cell. Proteomics MCP* **13:** 397–406

Farris JS (1977) Phylogenetic Analysis Under Dollo's Law. *Syst. Zool.* **26:** 77–88

Floor SN & Doudna JA (2016) Tunable protein synthesis by transcript isoforms in human cells. *eLife* **5:**

Gerstein MB, Rozowsky J, Yan K-K, Wang D, Cheng C, Brown JB, Davis CA, Hillier L, Sisu C, Li JJ, Pei B, Harmanci AO, Duff MO, Djebali S, Alexander RP, Alver BH, Auerbach R, Bell K, Bickel PJ, Boeck ME, et al (2014) Comparative analysis of the transcriptome across distant species. *Nature* **512:** 445–448

Gonzaga-Jauregui C, Lupski JR & Gibbs RA (2012) Human genome sequencing in health and disease. *Annu. Rev. Med.* **63:** 35–61

Graveley BR (2005) Mutually Exclusive Splicing of the Insect Dscam Pre-mRNA Directed by Competing Intronic RNA Secondary Structures. *Cell* **123:** 65–73

Graveley BR, Kaur A, Gunning D, Zipursky SL, Rowen L & Clemens JC (2004) The organization and evolution of the dipteran and hymenopteran Down syndrome cell adhesion molecule (Dscam) genes. *RNA* **10:** 1499–1506

Hammesfahr B & Kollmar M (2012) Evolution of the eukaryotic dynactin complex, the activator of cytoplasmic dynein. *BMC Evol. Biol.* **12:** 95

Hatje K, Hammesfahr B & Kollmar M (2013) WebScipio: Reconstructing alternative splice variants of eukaryotic proteins. *Nucleic Acids Res.* **41:** W504-509

Hatje K & Kollmar M (2013) Expansion of the mutually exclusive spliced exome in Drosophila. *Nat. Commun.* **4:** 2460

Hatje K & Kollmar M (2014) Kassiopeia: a database and web application for the analysis of mutually exclusive exomes of eukaryotes. *BMC Genomics* **15:** 115

Irimia M, Weatheritt RJ, Ellis JD, Parikshak NN, Gonatopoulos-Pournatzis T, Babor M, Quesnel-Vallières M, Tapial J, Raj B, O'Hanlon D, Barrios-Rodiles M, Sternberg MJE, Cordes SP, Roth FP, Wrana JL, Geschwind DH & Blencowe BJ (2014) A highly

conserved program of neuronal microexons is misregulated in autistic brains. *Cell* **159:** 1511–1523

Johansson JU, Ericsson J, Janson J, Beraki S, Stanić D, Mandic SA, Wikström MA, Hökfelt T, Ogren SO, Rozell B, Berggren P-O & Bark C (2008) An ancient duplication of exon 5 in the Snap25 gene is required for complex neuronal development/function. *PLoS Genet.* **4:** e1000278

Kaplan JM, Kim SH, North KN, Rennke H, Correia LA, Tong HQ, Mathis BJ, Rodríguez-Pérez JC, Allen PG, Beggs AH & Pollak MR (2000) Mutations in ACTN4, encoding alpha-actinin-4, cause familial focal segmental glomerulosclerosis. *Nat. Genet.* **24:** 251–256

Keller O, Odronitz F, Stanke M, Kollmar M & Waack S (2008) Scipio: using protein sequences to determine the precise exon/intron structures of genes and their orthologs in closely related species. *BMC Bioinformatics* **9:** 278

Kollmar M & Hatje K (2014) Shared Gene Structures and Clusters of Mutually Exclusive Spliced Exons within the Metazoan Muscle Myosin Heavy Chain Genes. *PLoS ONE* **9:** e88111

Kuhn M (2008) Building Predictive Models in R Using the caret Package. *J. Stat. Softw.* **28:** 1–26

Landrum MJ, Lee JM, Benson M, Brown G, Chao C, Chitipiralla S, Gu B, Hart J, Hoffman D, Hoover J, Jang W, Katz K, Ovetsky M, Riley G, Sethi A, Tully R, Villamarin-Salomon R, Rubinstein W & Maglott DR (2016) ClinVar: public archive of interpretations of clinically relevant variants. *Nucleic Acids Res.* **44:** D862-868

Lee C, Kim N, Roy M & Graveley BR (2010) Massive expansions of Dscam splicing diversity via staggered homologous recombination during arthropod evolution. *RNA* **16:** 91–105

Lee Y & Rio DC (2015) Mechanisms and Regulation of Alternative Pre-mRNA Splicing. *Annu. Rev. Biochem.* **84:** 291–323

Letunic I, Copley RR & Bork P (2002) Common exon duplication in animals and its role in alternative splicing. *Hum Mol Genet* **11:** 1561–1567

Li H, Handsaker B, Wysoker A, Fennell T, Ruan J, Homer N, Marth G, Abecasis G, Durbin R & 1000 Genome Project Data Processing Subgroup (2009) The Sequence Alignment/Map format and SAMtools. *Bioinformatics* **25:** 2078–2079

Lorenz R, Bernhart SH, Siederdissen CH zu, Tafer H, Flamm C, Stadler PF & Hofacker IL (2011) ViennaRNA Package 2.0. *Algorithms Mol. Biol.* **6:** 26

Matlin AJ, Clark F & Smith CWJ (2005) Understanding alternative splicing: towards a cellular code. *Nat. Rev. Mol. Cell Biol.* **6:** 386–398

Mayr JA, Zimmermann FA, Horváth R, Schneider H-C, Schoser B, Holinski-Feder E, Czermin B, Freisinger P & Sperl W (2011) Deficiency of the mitochondrial phosphate

carrier presenting as myopathy and cardiomyopathy in a family with three affected children. *Neuromuscul. Disord.* **21:** 803–808

Meijers R, Puettmann-Holgado R, Skiniotis G, Liu J, Walz T, Wang J & Schmucker D (2007) Structural basis of Dscam isoform specificity. *Nature* **449:** 487–491

Merkin J, Russell C, Chen P & Burge CB (2012) Evolutionary Dynamics of Gene and Isoform Regulation in Mammalian Tissues. *Science* **338:** 1593–1599

Nellore A, Jaffe AE, Fortin J-P, Alquicira-Hernández J, Collado-Torres L, Wang S, Phillips Iii RA, Karbhari N, Hansen KD, Langmead B & Leek JT (2016) Human splicing diversity and the extent of unannotated splice junctions across human RNA-seq samples on the Sequence Read Archive. *Genome Biol.* **17:** 266

Nilsen TW & Graveley BR (2010) Expansion of the eukaryotic proteome by alternative splicing. *Nature* **463:** 457–463

Pan Q, Shai O, Lee LJ, Frey BJ & Blencowe BJ (2008) Deep surveying of alternative splicing complexity in the human transcriptome by high-throughput sequencing. *Nat. Genet.* **40:** 1413–1415

Pillmann H, Hatje K, Odronitz F, Hammesfahr B & Kollmar M (2011) Predicting mutually exclusive spliced exons based on exon length, splice site and reading frame conservation, and exon sequence homology. *BMC Bioinformatics* **12:** 270

Pohl M, Bortfeldt RH, Grützmann K & Schuster S (2013) Alternative splicing of mutually exclusive exons--a review. *Biosystems* **114:** 31–38

Quinlan AR & Hall IM (2010) BEDTools: a flexible suite of utilities for comparing genomic features. *Bioinformatics* **26:** 841–842

Rogozin IB, Wolf YI, Sorokin AV, Mirkin BG & Koonin EV (2003) Remarkable Interkingdom Conservation of Intron Positions and Massive, Lineage-Specific Intron Loss and Gain in Eukaryotic Evolution. *Curr. Biol.* **13:** 1512–1517

Rose PW, Prlić A, Bi C, Bluhm WF, Christie CH, Dutta S, Green RK, Goodsell DS, Westbrook JD, Woo J, Young J, Zardecki C, Berman HM, Bourne PE & Burley SK (2015) The RCSB Protein Data Bank: views of structural biology for basic and applied research and education. *Nucleic Acids Res.* **43:** D345-356

Schmucker D, Clemens JC, Shu H, Worby CA, Xiao J, Muda M, Dixon JE & Zipursky SL (2000) Drosophila Dscam is an axon guidance receptor exhibiting extraordinary molecular diversity. *Cell* **101:** 671–684

Sharp PA & Burge CB (1997) Classification of introns: U2-type or U12-type. *Cell* **91:** 875–879

Sing T, Sander O, Beerenwinkel N & Lengauer T (2005) ROCR: visualizing classifier performance in R. *Bioinformatics* **21:** 3940–3941

Smith CWJ (2005) Alternative splicing--when two's a crowd. *Cell* **123:** 1–3

Sommer B, Keinänen K, Verdoorn TA, Wisden W, Burnashev N, Herb A, Köhler M, Takagi T, Sakmann B & Seeburg PH (1990) Flip and flop: a cell-specific functional switch in glutamate-operated channels of the CNS. *Science* **249:** 1580–1585

Splawski I, Timothy KW, Decher N, Kumar P, Sachse FB, Beggs AH, Sanguinetti MC & Keating MT (2005) Severe arrhythmia disorder caused by cardiac L-type calcium channel mutations. *Proc. Natl. Acad. Sci. U. S. A.* **102:** 8089-8096; discussion 8086–8088

Splawski I, Timothy KW, Sharpe LM, Decher N, Kumar P, Bloise R, Napolitano C, Schwartz PJ, Joseph RM, Condouris K, Tager-Flusberg H, Priori SG, Sanguinetti MC & Keating MT (2004) Ca(V)1.2 calcium channel dysfunction causes a multisystem disorder including arrhythmia and autism. *Cell* **119:** 19–31

Stanke M & Waack S (2003) Gene prediction with a hidden Markov model and a new intron submodel. *Bioinformatics* **19:** ii215-225

Sterne-Weiler T, Martinez-Nunez RT, Howard JM, Cvitovik I, Katzman S, Tariq MA, Pourmand N & Sanford JR (2013) Frac-seq reveals isoform-specific recruitment to polyribosomes. *Genome Res.* **23:** 1615–1623

Suyama M (2013) Mechanistic insights into mutually exclusive splicing in dynamin 1. *Bioinformatics* **29:** 2084–2087

Thierry-Mieg D & Thierry-Mieg J (2006) AceView: a comprehensive cDNA-supported gene and transcripts annotation. *Genome Biol.* **7 Suppl 1:** S12.1-14

Tilgner H, Knowles DG, Johnson R, Davis CA, Chakrabortty S, Djebali S, Curado J, Snyder M, Gingeras TR & Guigó R (2012) Deep sequencing of subcellular RNA fractions shows splicing to be predominantly co-transcriptional in the human genome but inefficient for lncRNAs. *Genome Res.* **22:** 1616–1625

Tress ML, Abascal F & Valencia A (2016) Alternative Splicing May Not Be the Key to Proteome Complexity. *Trends Biochem. Sci.*

UniProt Consortium (2015) UniProt: a hub for protein information. *Nucleic Acids Res.* **43:** D204-212

Wallace IM, O'Sullivan O, Higgins DG & Notredame C (2006) M-Coffee: combining multiple sequence alignment methods with T-Coffee. *Nucleic Acids Res.* **34:** 1692–1699

Wang ET, Sandberg R, Luo S, Khrebtukova I, Zhang L, Mayr C, Kingsmore SF, Schroth GP & Burge CB (2008) Alternative isoform regulation in human tissue transcriptomes. *Nature* **456:** 470–476

Wang J, Duncan D, Shi Z & Zhang B (2013) WEB-based GEne SeT AnaLysis Toolkit (WebGestalt): update 2013. *Nucleic Acids Res.* **41:** W77-83

Warde-Farley D, Donaldson SL, Comes O, Zuberi K, Badrawi R, Chao P, Franz M, Grouios C, Kazi F, Lopes CT, Maitland A, Mostafavi S, Montojo J, Shao Q, Wright G, Bader GD & Morris Q (2010) The GeneMANIA prediction server: biological network

integration for gene prioritization and predicting gene function. *Nucleic Acids Res*. **38:** W214-220

Weatheritt RJ, Sterne-Weiler T & Blencowe BJ (2016) The ribosome-engaged landscape of alternative splicing. *Nat. Struct. Mol. Biol.* **23:** 1117–1123

Xiong HY, Alipanahi B, Lee LJ, Bretschneider H, Merico D, Yuen RKC, Hua Y, Gueroussov S, Najafabadi HS, Hughes TR, Morris Q, Barash Y, Krainer AR, Jojic N, Scherer SW, Blencowe BJ & Frey BJ (2015) RNA splicing. The human splicing code reveals new insights into the genetic determinants of disease. *Science* **347:** 1254806

Xue Z, Huang K, Cai C, Cai L, Jiang C, Feng Y, Liu Z, Zeng Q, Cheng L, Sun YE, Liu J, Horvath S & Fan G (2013) Genetic programs in human and mouse early embryos revealed by single-cell RNA sequencing. *Nature* **500:** 593–597

Yan L, Yang M, Guo H, Yang L, Wu J, Li R, Liu P, Lian Y, Zheng X, Yan J, Huang J, Li M, Wu X, Wen L, Lao K, Li R, Qiao J & Tang F (2013) Single-cell RNA-Seq profiling of human preimplantation embryos and embryonic stem cells. *Nat. Struct. Mol. Biol.* **20:** 1131–1139

Yang Y, Sun F, Wang X, Yue Y, Wang W, Zhang W, Zhan L, Tian N, Shi F & Jin Y (2012) Conservation and regulation of alternative splicing by dynamic inter- and intra-intron base pairings in Lepidoptera 14-3-3ξ pre-mRNAs. *RNA Biol.* **9:** 691–700

Yates A, Akanni W, Amode MR, Barrell D, Billis K, Carvalho-Silva D, Cummins C, Clapham P, Fitzgerald S, Gil L, Girón CG, Gordon L, Hourlier T, Hunt SE, Janacek SH, Johnson N, Juettemann T, Keenan S, Lavidas I, Martin FJ, et al (2016) Ensembl 2016. *Nucleic Acids Res.* **44:** D710-716

Yura K, Shionyu M, Hagino K, Hijikata A, Hirashima Y, Nakahara T, Eguchi T, Shinoda K, Yamaguchi A, Takahashi K-I, Itoh T, Imanishi T, Gojobori T & Go M (2006) Alternative splicing in human transcriptome: functional and structural influence on proteins. *Gene* **380:** 63–71

Zhang JD, Hatje K, Sturm G, Broger C, Ebeling M, Burtin M, Terzi F, Pomposiello SI & Badi L (2017) Detect tissue heterogeneity in gene expression data with BioQC. *BMC Genomics* **18:** 277

Zubović L, Baralle M & Baralle FE (2012) Mutually exclusive splicing regulates the Nav 1.6 sodium channel function through a combinatorial mechanism that involves three distinct splicing regulatory elements and their ligands. *Nucleic Acids Res* **40:** 6255–6269

Figure legends

Figure 1 - The human genome contains 1399 high-confidence MXEs. A) Schematic representation of the various annotated and predicted exon types included in the MXE candidate list. For MXE validation at least three restraints must be fulfilled: the absence of an MXE-joining read (R1), except for those leading to frame shift, and the presence of two MXE-bridging SJ reads (R2 and R3). B) Prediction and validation of 1399 1SJ (855 3SJ) human MXEs. Top: Dataset of 6541 MXE candidates from annotated and predicted exons. Bottom left: MXE candidates for which splice junction data is currently missing hindering their annotation as MXE or other splice variant. Bottom right: Validation of the MXE candidates using over 15 billion RNA-seq reads. The outer circles represent the validation based on at least a single read for each of the validation criteria (1SJ), while the validation shown in the inner circles required at least three reads (3SJ). C) MXE saturation analysis. Whereas increasing amounts of RNA-seq reads should lead to the confirmation of further MXE candidates, more RNA-seq reads might also result in the rejection of previously validated MXEs. The green curves show the number of validated MXEs in relation to the percentage of total RNA-seq reads used for validation. The orange curves indicate the number of initially 'validated MXEs' that were rejected with increasing amounts of reads. Grey dashed lines indicate the point of saturation, which is defined as the point where a two-fold increase in reads leads to rejection of less than 1% of the validated MXEs. Of note, whereas the rejection of validated MXEs saturates with 20% of the data the amount of novel MXE validations is still rapidly increasing. D) Distribution validated MXEs in two-exon and multi-exon clusters. E) Size and distribution of multi-cluster MXEs. F) Mutually exclusive splicing of the *CUX1* gene (cut-like homeobox 1) requires at least three levels of regulation to ensure that only a single exon of each cluster is included in each transcript and to provide tissue, cell-type and developmental stage specificity.

Figure 2 – MXE presence is regulated at the RNA and protein folding level. A) Schematic representation of MXE splicing regulation via splice-site incompatibility, branch point proximity, and translational frame shift leading to NMD. B) Observed usage of MXE splicing regulation in 629 MXE clusters. C) By mutually exclusive inclusion into transcripts, MXEs of a cluster are supposed to encode the same region of a protein structure. If the respective regions of the protein structures are embedded within secondary structural elements (the ends of the exon-encoded peptides are part of α-helices and/or β-strands), it is highly unlikely that the translation of a transcript will result in a folded protein in case the respective exon is missing (skipped exon). If the MXEs have highly similar sequences and do not encode repeat regions, it seems unlikely that both could be present in tandem or absent at all in a folded protein. Here, we have combined protein structure features (colours) with splicing regulation information (symbols). Accordingly, 87% of the MXE encoded protein regions are embedded in secondary structural elements (orange and green symbols), and most of the remaining MXEs can only be spliced mutually exclusive because splicing as differentially included exons would lead to frame shifts (blue circles). As examples, we labelled many MXE clusters distinguishing annotated MXEs (purple letters), known exons that we validated as MXEs (orange letters), and clusters containing novel exons (dark-grey letters).

Figure 3 – MXE expression is tightly regulated across tissues and development. A) Heatmap showing all differentially expressed MXE clusters with at least 3 RPKM. Here, we used the Gini coefficient, which is a measure of the inequality among values of a frequency distribution (Ceriani & Verme, 2012) and has successfully been used to determine tissue-enriched gene sets (Zhang *et al*, 2017), to determine highly tissue-specific MXEs (maximum

normalized Gini index of cluster) and MXEs with a broad tissue expression distribution (minimum Gini index). For each MXE cluster the expression of the specific MXE (maximum Gini index of cluster) is subtracted from the expression of the ubiquitous MXE (minimum Gini index) and scaled between -1 (broad tissue distribution) and 1 (highly tissue specific). Each column represents an MXE pair and each row represents MXE expression in a tissue, cell-type, or at a developmental time point. The bar graph summarizes counts where the specific MXE is 1.5 fold more expressed than the ubiquitous MXE. B) Overview of differentially expressed genes for the Embryonic Development, ENCODE, and Human Protein Atlas datasets. C) Overview of differentially expressed MXEs for the Embryonic Development, ENCODE, and Human Protein Atlas datasets.

Figure 4 – MXE-ratio expression predicts disease pathology. A) 35 MXE clusters contain 82 pathogenic mutations causing neurologic (10), neuromuscular (7), cardiac (6), cancer (3), or other diseases (9). B) Sashimi plots showing exon as well as splice junction reads (including number of reads) in kidney and heart for *SLC25A3*. C) Heatmap showing the expression difference of MXE clusters containing pathogenic SNPs scaled between -1 and 1 (blue = high expression non-SNP containing MXE, red = high expression SNP-containing MXE). Columns represent MXE clusters and rows tissues, cell types, and developmental stages. The column bar graph summarizes counts where the SNP-containing MXE is 1.5 fold more expressed than the non-SNP containing MXE, whereas the column bar graph shows this for each tissue, cell type, and developmental stage. D) Receiver operating characteristic (ROC) curve showing true and false positive rates for cardiomyopathy-neuromuscular disease prediction based on spatio-temporal MXE expression.

Figure 5 – Rapid MXE gain and loss in mammalian evolution

Validated MXE clusters were sorted by chromosome and chromosomal position. Outer circles show the annotation of each exon as MXE in Ensembl and Aceview, and the annotation as exon in Ensembl as indicated by the legend. The lengths of the bars denote the percentage of matching exons for each cluster. For comparison, we show the annotation as MXE in two different Ensembl versions highlighting the dynamics of exon annotations over time. The comparison of the GenBank with the latest Ensembl annotation (v. 37.75) showed considerably less exons annotated as MXEs (58) in Ensembl although these include six of the 'novel exons' (Supplementary Fig. S1). The presence of the respective validated MXEs in each of the analysed 18 mammals is shown by coloured bars. The 18 mammals, their phylogenetic relation and the total numbers of MXEs shared with human are presented at the bottom. The innermost circle represents the number of exons within each cluster of MXEs.

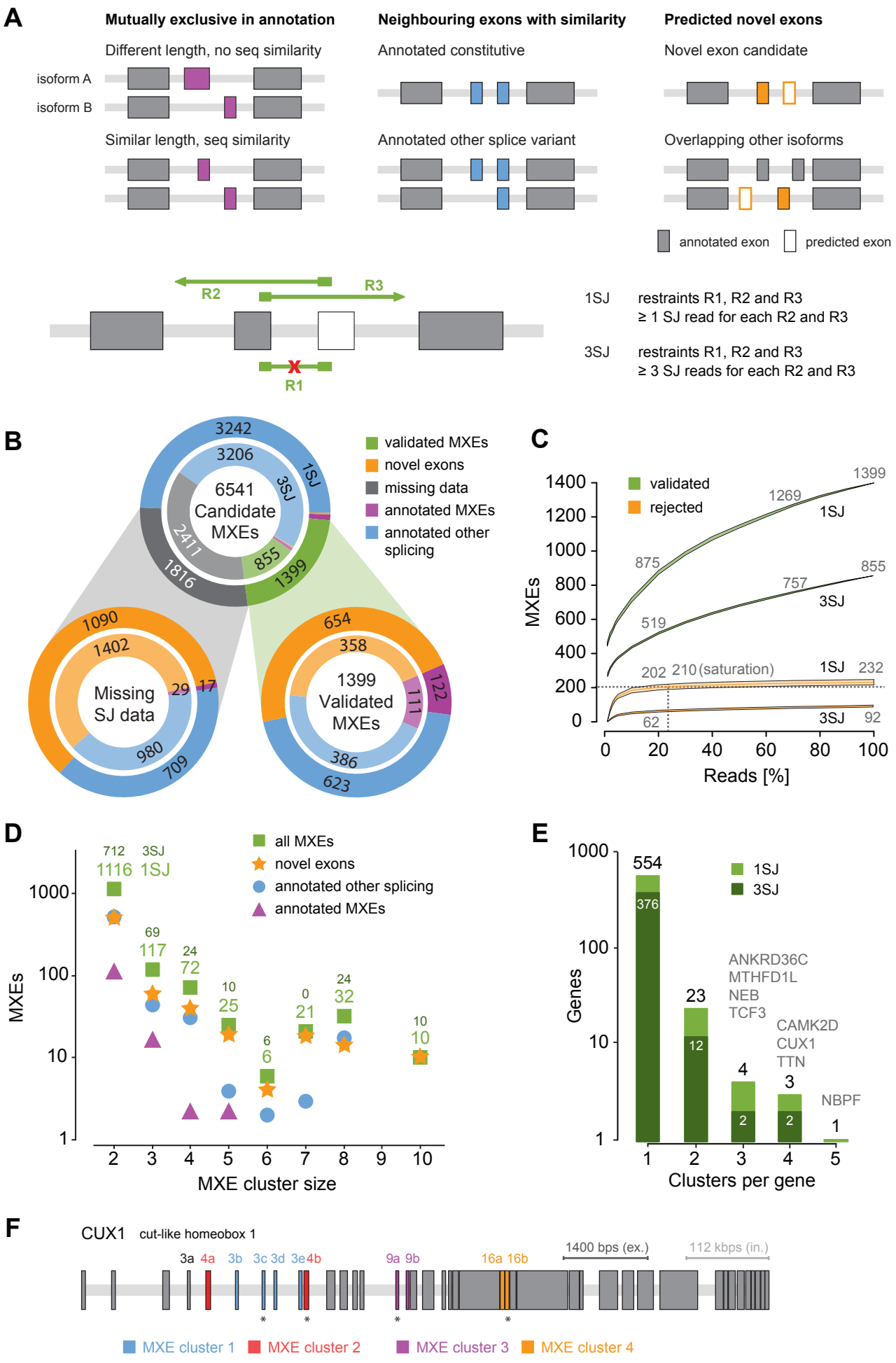
A
Mutually exclusive in annotation
Different length, no seq similarity
isoform A
isoform B
Similar length, seq similarity
Neighbouring exons with similarity
Annotated constitutive
Annotated other splice variant
Predicted novel exons
Novel exon candidate
Overlapping other isoforms
annotated exon
predicted exon
R1
R2
R3
1SJ restraints R1, R2 and R3
≥ 1 SJ read for each R2 and R3
3SJ restraints R1, R2 and R3
≥ 3 SJ reads for each R2 and R3
B
validated MXEs
novel exons
missing data
annotated MXEs
annotated other splicing
6541 Candidate MXEs
3242
3206
1SJ
3SJ
2411
1816
855
1399
Missing SJ data
1090
1402
29
17
980
709
1399 Validated MXEs
654
358
122
111
386
623
C
validated
rejected
MXEs
Reads [%]
1399
1269
1SJ
875
855
757
3SJ
519
202
210 (saturation)
1SJ
232
62
3SJ
92
D
all MXEs
novel exons
annotated other splicing
annotated MXEs
MXEs
MXE cluster size
712
1116
3SJ
1SJ
69
117
24
72
10
25
6
6
0
21
24
32
10
10
E
1SJ
3SJ
Genes
Clusters per gene
554
376
23
12
4
2
3
2
1
ANKRD36C
MTHFD1L
NEB
TCF3
CAMK2D
CUX1
TTN
NBPF
F
CUX1 cut-like homeobox 1
3a 4a 3b 3c 3d 3e 4b 9a 9b 16a 16b
1400 bps (ex.)
112 kbps (in.)
MXE cluster 1
MXE cluster 2
MXE cluster 3
MXE cluster 4

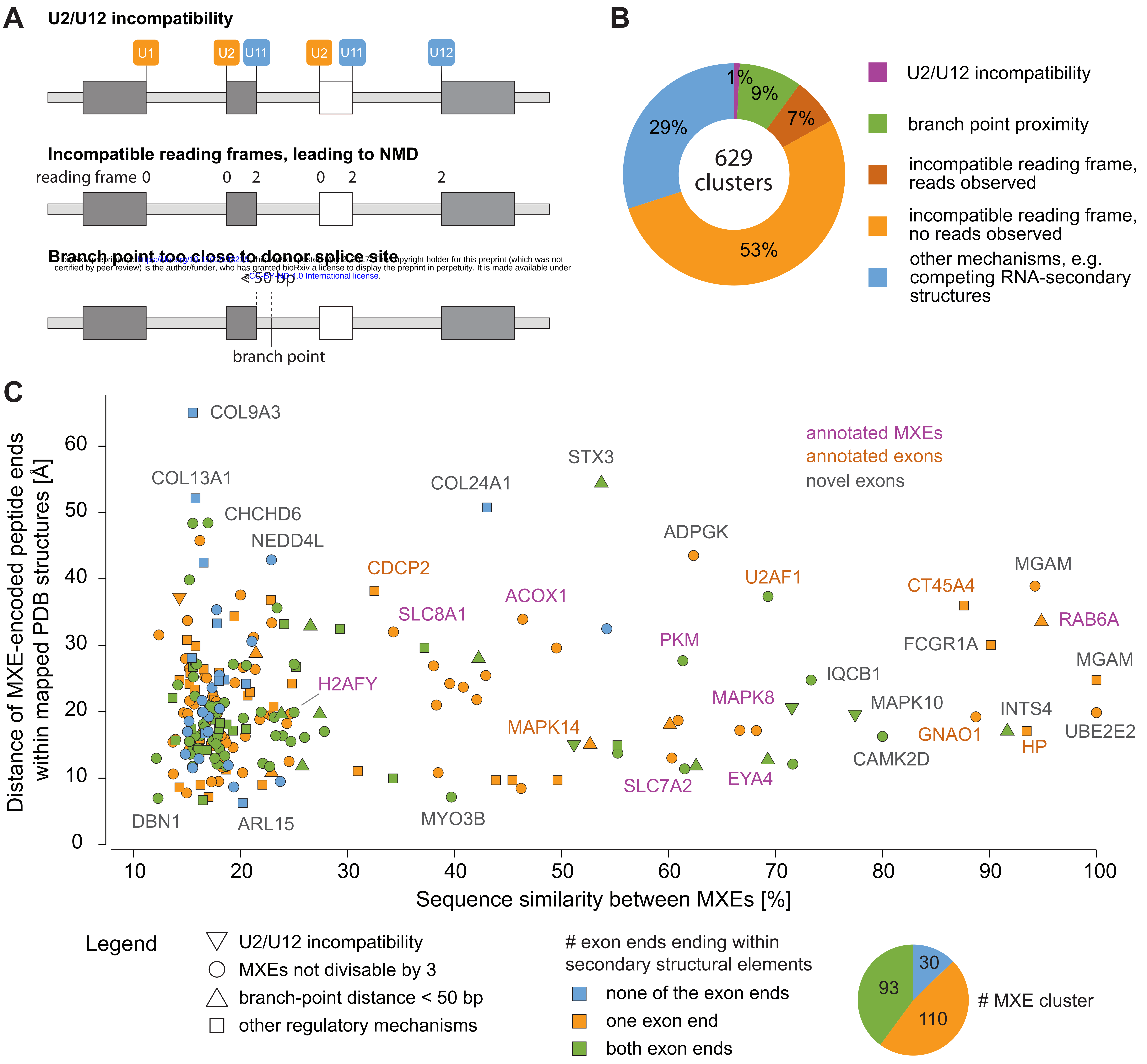

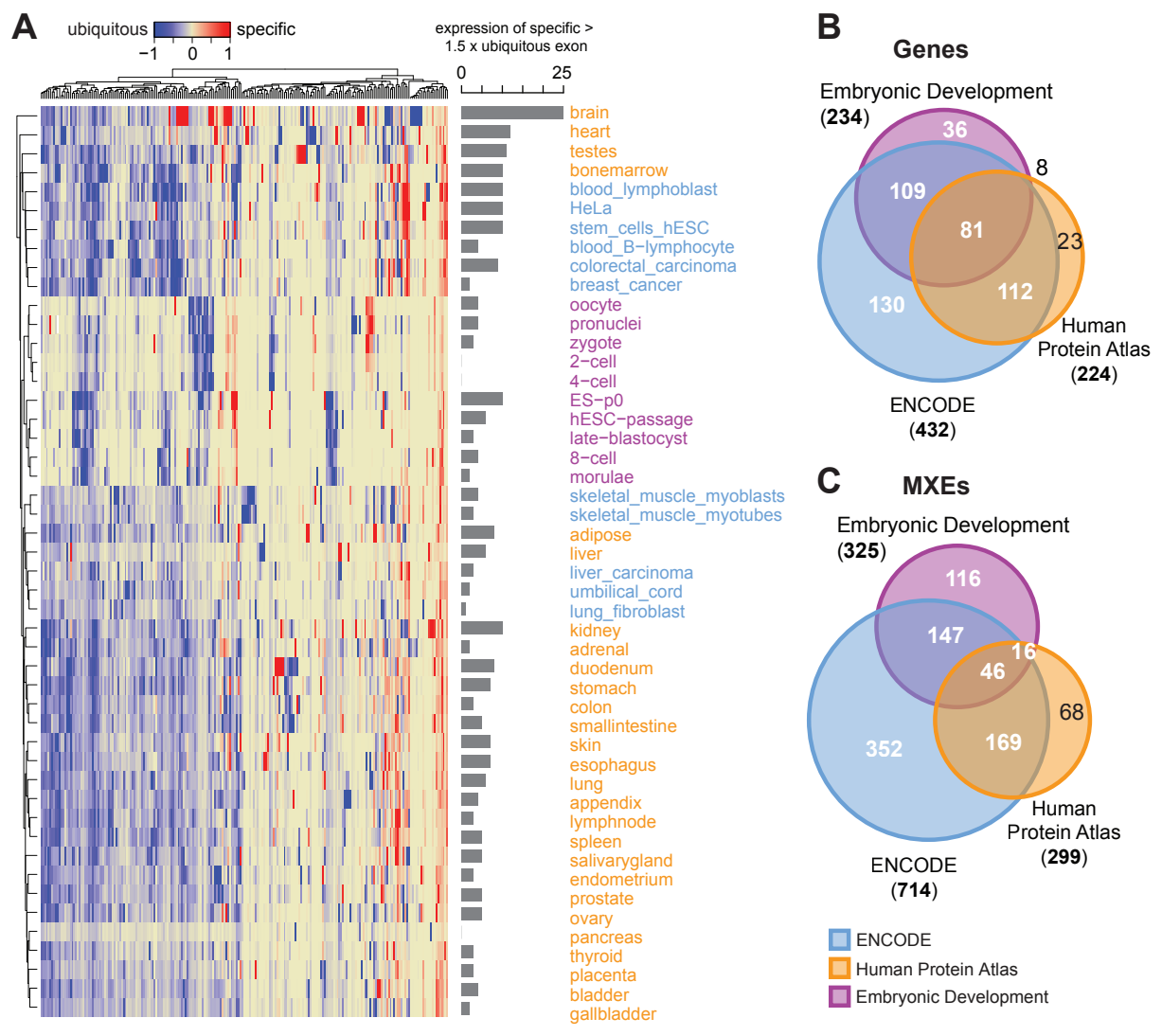
A
ubiquitous
specific
−1
0
1
expression of specific >
1.5 x ubiquitous exon
0
25
brain
heart
testes
bonemarrow
blood_lymphoblast
HeLa
stem_cells_hESC
blood_B−lymphocyte
colorectal_carcinoma
breast_cancer
oocyte
pronuclei
zygote
2−cell
4−cell
ES−p0
hESC−passage
late−blastocyst
8−cell
morulae
skeletal_muscle_myoblasts
skeletal_muscle_myotubes
adipose
liver
liver_carcinoma
umbilical_cord
lung_fibroblast
kidney
adrenal
duodenum
stomach
colon
smallintestine
skin
esophagus
lung
appendix
lymphnode
spleen
salivarygland
endometrium
prostate
ovary
pancreas
thyroid
placenta
bladder
gallbladder
B
Genes
Embryonic Development
(234)
36
8
109
81
23
112
130
Human
Protein Atlas
(224)
ENCODE
(432)
C
MXEs
Embryonic Development
(325)
116
147
16
46
68
352
169
Human
Protein Atlas
(299)
ENCODE
(714)
ENCODE
Human Protein Atlas
Embryonic Development

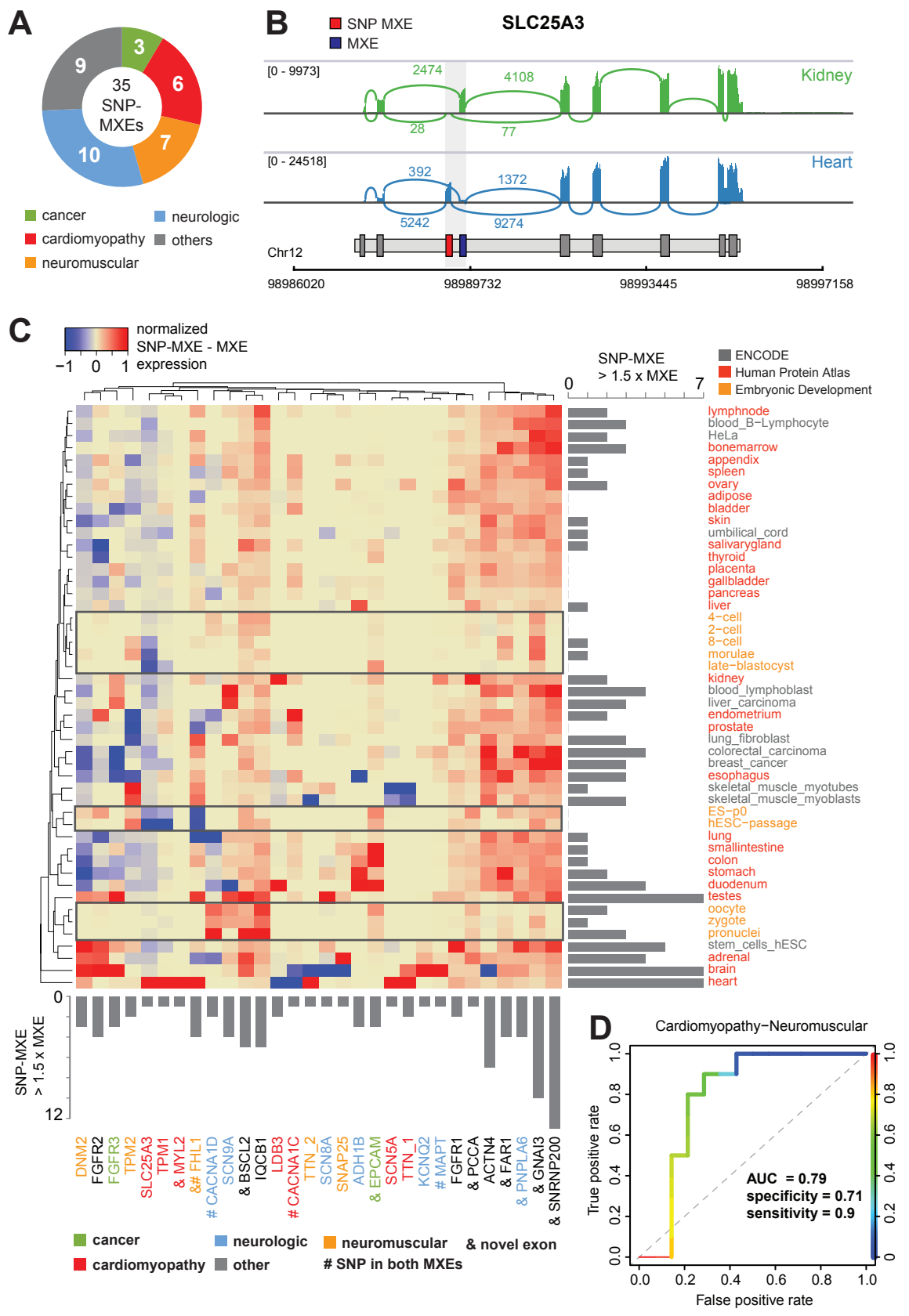
A
35 SNP-MXEs
3
6
7
10
9
cancer
cardiomyopathy
neuromuscular
neurologic
others
B
SNP MXE
MXE
SLC25A3
[0 - 9973]
2474
4108
28
77
Kidney
[0 - 24518]
392
1372
5242
9274
Heart
Chr12
98986020
98989732
98993445
98997158
C
normalized SNP-MXE - MXE expression
−1 0 1
SNP-MXE > 1.5 x MXE
0
7
ENCODE
Human Protein Atlas
Embryonic Development
lymphnode
blood_B−Lymphocyte
HeLa
bonemarrow
appendix
spleen
ovary
adipose
bladder
skin
umbilical_cord
salivarygland
thyroid
placenta
gallbladder
pancreas
liver
4−cell
2−cell
8−cell
morulae
late−blastocyst
kidney
blood_lymphoblast
liver_carcinoma
endometrium
prostate
lung_fibroblast
colorectal_carcinoma
breast_cancer
esophagus
skeletal_muscle_myotubes
skeletal_muscle_myoblasts
ES−p0
hESC−passage
lung
smallintestine
colon
stomach
duodenum
testes
oocyte
zygote
pronuclei
stem_cells_hESC
adrenal
brain
heart
SNP-MXE > 1.5 x MXE
0
12
DNM2
FGFR2
FGFR3
TPM2
SLC25A3
TPM1
& MYL2
&# FHL1
CACNA1D
SCN9A
& BSCL2
IQCB1
LDB3
CACNA1C
TTN_2
SCN8A
SNAP25
ADH1B
& EPCAM
SCN5A
TTN_1
KCNQ2
MAPT
FGFR1
& PCCA
ACTN4
& FAR1
& PNPLA6
& GNAI3
& SNRNP200
cancer
cardiomyopathy
neurologic
other
neuromuscular
& novel exon
# SNP in both MXEs
D
Cardiomyopathy−Neuromuscular
True positive rate
False positive rate
0.0
0.2
0.4
0.6
0.8
1.0
AUC = 0.79
specificity = 0.71
sensitivity = 0.9